Reservoir Characterization and Simulation of an Oligocene-Miocene Isolated Carbonate Platform: Banyu Urip Field, East Java Basin, Indonesia*

Toni Simo[1], Rizky P. Sekti[2], Fikril Hakiki[2], Michael Sun[2], Rodrick D. Myers[1], and Shawn Fullmer[1]

[1]ExxonMobil URC, Houston, TX toni.t.simo@exxonmobil.com
[2] Mobil Cepu LTD, Jakarta, Indonesia

Regional Geology, East Java Basin

Through the Cenozoic, Southeast Asia accumulated extensive sedimentary deposits that reflect active tectonics and environmental change, such as closure of the tropical Indonesian seaway and development of the Indonesian through-flow. The sedimentary fill in the East Java basin reflects the relative influence of regional and local tectonics, sea level variations, weathering of land masses, and influx of clastics. The East Java basin constitutes a part of the Southeast Asia Tertiary petroleum system, which owes its origin to Eocene - Oligocene extensional tectonics and deposition of thick syn- and post-rift lacustrine organic-rich shale (Bransden and Matthews, 1992; Cole and Crittenden, 1997) and contains significant hydrocarbon resource accumulations in Tertiary carbonates and clastics (Najoan, 1972).

The onshore East Java Basin is traditionally subdivided into four, E-W, trending tectono-stratigraphic domains (Van Bemmelen 1949; Figure 1). From N-S they are:
1. Rembang Zone of predominantly 'shelfal' Oligocene-Recent sediments, with common young inversion anticlinal structures verging to the south. The southern part with less topographic relief has been called „Randublatung zone."
2. Kendeng Zone: thick, predominantly deep-water Miocene to Pliocene-Pleistocene sediments, major negative gravity anomaly, and with young thrusting and folding verging to the north.
3. Modern Volcanic Arc: with most activity primarily latest Pliocene- Recent.
4. Southern Mountains: a south-dipping monocline, with outcrops of Eocene sandstones, latest Oligocene- earliest Miocene arc volcanics, and middle-late Miocene carbonates. This area was apparently exposed and a sediment source during much of the later middle Miocene - Pliocene and underwent recent uplift

The Tertiary stratigraphic record of the East Java Basin suggests periods of relative quiescence alternating with periods of tectonic activity (Figure 2). Times of increased volcanism, folding/faulting and the development of unconformities include: Middle Eocene extension phase

with WSW-ENE-trending horsts and grabens; Oligocene - mid-Miocene sag subsidence phase with fragmentation of the shallow water and generalized deepening; mid- to late Miocene inversion of Rembang area; and mddle Miocene uplift of Borneo and influx of clastics; late Miocene (~7 Ma) to Pleistocene inversion of the basin.

The Cepu Block is located in the Randublatung zone between the Rembang and Kendeng zones. In this area, grabens generated during the Eocene extensional phase were filled with fluvial, lacustrine, and marginal marine sediments. Late Eocene and Oligocene shallow-water marine carbonates developed concurrently with and following graben fill over the broad and somewhat irregularly inundated highs, producing areally extensive shallow-water carbonate platforms surrounded by deep-water carbonates.

Figure 3 illustrates the main stratigraphic units in the Cepu block, the position of reservoir horizons in some of the main oil and gas fields in the area (Soeparyono and Lennox, 1989), and the main structural events. The carbonate system in the Cepu area represents continuous, but punctuated deposition from the late Eocene (Priabonian) to middle Miocene (Langhian), reflecting tectonically influenced subsidence associated with loading from the volcanic arc to the south. Superimposed on this trend, the eustatic overprint appears to control the geometry of the buildups whereas significant backsteps or changes in stacking patterns can be tied to major eustatic falls in sea level during the Rupleian1, Chattian1, Aquitanian1 and Bur5/Lan1. The onset of carbonate deposition varies across the region dependent on structurally controlled antecedent topography on which the initial carbonate shoals nucleated. The seismic surface that represents the base carbonate envelope is therefore diachronous. Localized shoals were deposited on local highs associated with horst blocks over a broad platform with seaways in-between (see Van Simaeys et. al., 2011). Irregularities of the flooded landform and differential subsidence created variability in thickness and facies across the Cepu high. The depositional geometries are generally aggradational and result in a sub-parallel seismic expression over much of the depositional area. Seismic geometries and isochrons of the carbonate section indicate that sediment thickness was greater at the margins of the platform. Thick calciturbidites and debrites accumulated concurrently in the basin (Apotria et. al., 2009).

Middle and end-Rupelian times are marked by evidence for physical and chemical erosion, indicating widespread exposure. Flooding followed exposure; shallow-water carbonate deposition occupied a smaller are,a and platforms occasionally drowned.

Following development of the major mid-Oligocene unconformity, the carbonate system of Cepu began to undergo significant transformation. Increasing accommodation (a combination of continued rapid subsidence and the major sea-level transgression of the late Oligocene) forced the carbonate factory to backstep to small areas over the pre-existing highs. These highs generally coincide with the older margins of the platform, although some minor, short-lived buildups were established in seaways. Backstepping was followed by an aggradational phase during the Chattian-Burdigalian. Multiple lowstand-exposure and transgressive-deepening periods from the Aquitanian to Langhian resulted in successive exposure of the buildups, reestablishment of the in situ shallow-water carbonate system, and finally cessation of carbonate deposition. The effect of accommodation (mainly subsidence) was different across the different platforms, causing drowning at different times. In general the carbonate buildups are younger towards the northeast. This trend can be attributed to increasing subsidence westward such that the buildups were able to keep up and remain in the photic zone longer before they were eventually overwhelmed by clastic influx. Concurrent with deposition of the shallow-water carbonate buildups, sedimentation on the flanks was characterized by deep-water marls and calciturbidites and carbonate debrites.

Deposition in the Cepu high-block changed from carbonates to siliciclastics during the Burdigalian-Langhian transition (Ardhana, 1993). A system of north-to-south prograding slope and prodelta deposits filled and covered the topography left by drowned buildups in the Langhian and early Tortonian. Minor south-verging thrust faults are post-dated by Langhian sandstones, constraining the initiation of contraction in the Cepu (Rembang) area within the Langhian. During the late Tortonian, the water depth increased and deep-water shale was deposited. The latest Miocene is characterized by a change to deep-water carbonate (chalks and calciturbidites) and shale deposition. A major, tectonically enhanced unconformity separates the Miocene from the Plio-Pleistocene, which is characterized by a syn-tectonic succession of volcaniclastic sandstones, shale, and shallow-water carbonates around actively growing anticlines. During the Zanclean the area became a contractional setting, with thrusting and associated folds controlling the distribution of sediment.

Cepu Block

A significant amount of hydrocarbon accumulation has been discovered from the Tertiary Cepu carbonate platform archipelago. These oil and gas discoveries in the block include more than 8 isolated carbonate platforms (with similar growth history but different demise times and reservoir properties) and younger, deep-water siliciclastic reservoirs (Figure 4). The well and seismic data indicate that the carbonate reservoir is better defined, more productive, and larger than the sandstone reservoir (Figure 5).

The emphasis of this core workshop is the main carbonate oil field called Banyu Urip. Seven wells have been drilled to appraise the field, and a 3-D seismic survey was acquired over the southeastern half of the Cepu Block (1213 square kilometers). The Banyu Urip carbonate reservoir is a steep-flanked carbonate buildup with approximately 3300 ft of relief relative to the surrounding equivalent basin strata. The carbonate reservoir is approximately 2500 acres in area. Of the seven wells drilled, six penetrated the carbonate and confirmed oil, the seventh well was drilled to target the clastic reservoir (Figure 6). The focus of initial development plan is a full-reservoir development of the carbonate reservoir supplemented with clastic oil production wells. The carbonate reservoir will be developed with an anticipated 30 production wells, with average well spacing of 55 acres. Injection water is designed to replace reservoir voidage (produced hydrocarbons and water) and will require a total of 13 wells. Produced gas will be re-injected via two gas injection wells. Early clastic production will be initiated from future oil production wells. An Early Production Facility project began in 3Q, 2008. The production scope included 4 existing wells as oil producers, 1 well as a water injector and 1 well as a gas injector. The production performance was monitored closely through real-time data collection system. In addition, 4 wells were installed with permanent downhole pressure monitoring system. As of 2Q, 2011, the well performance, field production and pressure agreed well with model forecast.

Facies, Diagenesis and Reservoir Properties

The stratigraphic and diagenetic complexities inherent in carbonate reservoirs require accurate reservoir descriptions and models to optimize the production recovery. Facies, diagenesis, and distribution of the related reservoir properties are key to characterize the reservoirs. The objective of this section is to establish detailed analysis of facies types and related diagenesis, and to constrain high-resolution sequence stratigraphy and cyclicity.

The lithofacies analysis is based on 2000 feet of core from 5 wells. The core analysis is based on several key observations, such as sedimentary texture, grain type, sedimentary structure, facies boundary, diagenesis, and pore type.

Lithofacies and Sequences

Based on the seismic data interpretation of Banyu Urip, the lower Miocene strata can be divided into an early aggrading phase and later retrograding phase (Figure 7).

The aggrading phase contains the following lithofacies (Figure 8):
1. Coral Boundstone/Coral Rudstone: includes massive coral framestone and branching coral framestone.
2. Patchy Cemented (rich/poor) Skeletal Packstone: consists of coral packstone matrix with some randomly distributed patchy cemented grains. The abundance of the patchy cement is unpredicted. This facies composes the major proportion of rock within the platform interior aggrading phase
3. Coral Floatstone – Coral Rudstone: coral rich facies with packstone–grainstone matrix.
4. Skeletal Packstone–Grainstone.
5. Skeletal Wackestone–Packstone.
6. Echinoid Wackestone–Packstone.

The lithofacies in the aggrading phase are arranged in shallowing-upward sequences often capped by exposure surface. Figure 9 shows two styles of sequences; one near the platform margin and the other in the platform interior. Key differences are the abundance of corals near the margin and the presence of echinoid-rich wackestone-packstone in the interior. Generally, the sequences are asymmetric with skeletal grain-supported bases and coral-rich tops. Few sequences in the interior are almost asymmetric with a fining-upward base and a coarsening-upward top (Figure 9).

The lithofacies in the retrograding phase (Figure 10 and 11) consist of:
1. Platy Coral bafflestone: consists of platy coral and delicate finger corals. It is interpreted as slightly deeper water environment compared to the massive and branching coral framestone.
2. Rhodolith Floatstone: high energy environment.
3. Platy red algae floatstone: thin-platy red algae-rich facies.

The main characteristic of this phase is the increase of the red algae and a decrease of corals. The abundance of red algae suggests that the depositional environment shifted into more stressful environment for corals. The lithofacies succession is arranged into shallowing-upward successions with red algae-rich bases and grain-supported tops with platy coral-rich-caps and occasionally coral-rich lithologies (Figure 10). Facies variability is much higher than in the aggrading facies and more difficult to predict.

Diagenesis

The characteristic of the Banyu Urip reservoir is the porosity/permeability trends of the aggrading and retrograding phases ([Figure 12](#)). The aggrading phase has high permeability and porosity and is grouped towards the high-end ([Figure 12](#)), while the retrograding phase has a linear relationship ([Figure 12](#)). The trends highlight the importance of diagenesis (aggrading phase) and facies (retrograding phase) in the reservoir. [Figure 13](#) illustrates the differences in a well located in the platform interior.

A qualitative petrographic analysis of thin sections from the wells in Banyu Urip field was performed to characterize the diagenetic history and reservoir quality of the carbonate section. Platform interior areas at Banyu Urip experienced typical early marine diagenesis and abundant, exposure-related, fresh-water diagenesis. Later diagenesis included multiple episodes of dissolution by hydrothermal fluids and precipitation of a host of different burial cements ([Figure 14](#)).

The resultant pore system is a combination of primary interparticle pores, secondary moldic pores, secondary micro-pores, and secondary touching vugs. Micro-pores and touching vugs in the form of connected molds and fracture connected vugs appear to be the most prevalent components of the pore system and are the dominant influence on reservoir quality. Lateral and vertical distribution of rock types with similar reservoir quality appears to correspond with facies and exposure surfaces. Later hydrothermal fluids flowed through the existing pore system and caused significant dissolution which enhanced overall connectivity. The complexity of the pore system has impact on field development and reservoir performance in the following ways:
1) Excess permeability or mega-porosity zones exist in areas where intense karsting occurred and later affected by hydrothermal fluid flow that was more intensely focused. These zones may facilitate early water or gas breakthrough, represent potential perforation clogging, and potential hazards for drilling
2) The close juxtaposition of touching vugs and microporous matrix may behave as a dual permeability system with significantly higher permeability in the touching vugs. It is unclear what the hydrocarbon-displacement efficiency will be from the micro-pore portion of the system and how that efficiency might be influenced by different-displacement strategies.

[Figure 14](#) shows the paragenetic sequence observed in the Banyu Urip reservoir. Following deposition, grains were micritized by boring organisms, and in a few instances coral was leached shortly thereafter, evidenced by sediment-filled corallite molds with micrite rims. Minor fibrous to bladed isopachous and microbial-related cementation occurred in the marine environment. Exposure of the system resulted in alteration and neomorphism related to surface processes and fabric-destructive dissolution and collapse related to karst development. Local vadose cementation is evident in a few, temporally distinct, grain-dominated, sequences. Isopachous blocky calcite cements on grain margins indicate initial cementation in the freshwater phreatic environment. Fabric inversion and continued blocky calcite cementation of inverted fabrics (molds filled with phreatic cements) illustrate continued pore-space evolution, and prolonged residence time, in the fresh-water phreatic zone. The saturation state with respect to calcite in a fresh-water lens is influenced by many variables but tends to evolve toward higher saturation with longer residence time, hence a transition from more dissolution to more cementation as the lens matures. However, pervasive fresh-water phreatic cementation is not as common as early leaching throughout the reservoir. It is difficult to explain this observation with diagenesis in a fresh-water lens alone. The mixing zone environment, attached to the base of every fresh-water lens,

has been recognized as a site of significant dissolution in modern carbonate platforms (Smart et al., 1998). It is plausible that a significant proportion of early leaching at Banyu Urip occurred in the mixing zone. The geometry of the mixing zone will tend to mimic the geometry of the base of the fresh-water lens, and the position of the mixing zone will fluctuate both laterally and vertically with the position of the fresh-water lens. It follows then that as relative sea-level fluctuates and the platform subsides any given stratigraphic position could pass through the mixing zone multiple times. Syntaxial overgrowths on echinoid fragments develop concomitantly with the marine and phreatic cements.

The relative timing of diagenetic events that occurred in the shallow burial environment is well constrained through cross-cutting relationships. Aragonite leaching and recrystallization continued throughout the early phase of diagenesis and into the shallow-burial phase. Mold-lining micritic rims are often all that remain of leached allochems, and in some cases molds have collapsed leaving a detritus of micritic rim debris as the only indication of a former moldic texture. Mechanical compaction due to burial is often the driving force behind mold collapse and is also evidenced by grain breakage, cement spalling, and fracturing. Stabilization of micritic material (microporosity evolution) is inferred but was not directly observed. Localized matrix dolomitization is observed in the platform interior. The dolomitization took place after allochem dissolution and local pore occlusion by coarse calcite but before chemical compaction. The shallow-burial interpretation for the dolomitization event is based on the assumption that stylolites that cut the dolomite rhombs are burial-related rather than tectonic in origin. Chemical compaction and stylolitization mark the transition from shallow to deeper burial processes in the reservoir.

Late, deeper burial, diagenesis is constrained by cross cutting relationships but is not tied to burial history or geochemical data. It consists of stylolitization, dolomitization, barite and calcite cementation, chemical compaction, various forms of clay, silica and pyrite cementation and carbonate dissolution events. Some compaction related fracturing is also observed along stylolites. Stylolites and stylo-related cements are leached by the first of several late dissolution events. Coarse calcite, saddle dolomite, and rare barite are precipitated in vugs and solution enhanced fractures associated with the first dissolution event. Barite and saddle dolomite precipitation indicates that the fluids responsible for the dissolution and dolomite cement precipitation are hydrothermal. The dolomite and calcite cements are in turn leached by a second late dissolution event and kaolinite cement is emplaced. The kaolinite is leached by a third dissolution event. The pore space associated with this event remains open. Throughout the episodic hydrothermal leaching the pore system continues to be solution enhanced, the microcrystalline matrix is leached and stable red algal and large benthic foraminifera grains are corroded. Late cements are observed throughout the section but tend to be more pervasive higher in the reservoir. Hydrocarbon charge is indicated as the final phase in the diagenetic sequence of events, based on the assumption that emplacement of hydrocarbons and displacement of formation water limit the water-rock interactions needed for diagenesis to occur.

Reservoir Quality Controls

The reservoir quality in Banyu Urip is influenced mostly by diagenesis. The significant differences in reservoir properties between the backstepping and aggrading phases are due to different diagenetic processes (Figure 15). The extensive early- and late-dissolution events enhance the initial pore system in the reservoir rock within the aggrading phase. In other words, it appears that once porosity and permeability are created by depositional and early diagenetic processes, fluids will continuously move though the same network of pores as a

positive feedback-loop. On the other hand, the backstepping phase has less influence of both early and late dissolution; the fresh-water diagenesis residence time is much less. Thus, there is no secondary porosity creation to be used by later diagenetic fluids. Thus the reservoir quality is more controlled by primary porosity within facies. One difference is the presence of coral.

Natural Fractures

Cepu carbonate platforms commonly contain natural fractures; their abundance and degree of opening can vary significantly across any given platform. Where these fractures have open aperture, either through preserved uncemented openings or cement dissolution along fracture planes, they can have an impact on reservoir porosity and permeability. Where fractures are abundant, they can provide flow pathways independent of the host-rock porosity or permeability. Potential effects of natural fractures on well performance have been observed in early well tests in Cepu reservoirs; these include 1) very high initial flow rates, 2) unexpected drilling fluid losses, 3) permeability anisotropy, and 4) significant flow heterogeneities in wells in close proximity. In order to better predict these potential effects field-wide and to better understand observed flow history, it is important to gain early insight into the fracture characteristics and their connectivity in the carbonate buildup and how these properties pertain to flow.

Direct observations of natural fractures from cores through Cepu carbonate buildups show a wide range of sizes, types, and relative timing. A systematic approach to capture fracture information is based on direct observations and image logs, when available. At Banyu Uript oil-based drilling muds were used which limited the usefulness of image logs; so the study was heavily dependent upon structural logging of conventional cores. The detailed core-logging procedure involves collecting information on individual fractures and attempting to relate these characteristics to fracture controls. Cepu core fracture logs include fracture location, type, dimensions, orientation, terminations, aperture sizes, cement types, and degree of fill. Once collated, these data are analyzed in the context of stratigraphic and structural position (proximity to faults, back-reef shoal, etc.), lithofacies type, and general rock properties.

Fracture information collected from three wells (312m/1025ft of core) are used to draw conclusions about fracture timing, causes and potential-flow impact. A few key observations about fracture timing, controls, and aperture provide the greatest insight into potential fracture flow in Cepu because they give insight into fracture connectivity and permeability. The core observations show there are a least four distinct fracture-timing events, determined by cross-cutting relationships. These sets, "dated" relative to stylolite formation (Figure 16), are:
- Set 1 – Opening-mode-only fractures, rarely observed and always 100% filled by diagenetic calcite.
- Set 2 – Fractures are also exclusively opening-mode, though they are syn-stylolitic and common. They are typically limited to 2 to 3 cm in length and confined between adjacent stylolites. Their apertures are commonly solution-enhanced and expected to contribute significantly to local permeability, but as a matrix enhancement only, due to limited connectivity across major stratigraphic boundaries.
- Set 3 – Fractures are predominantly opening-mode though sometimes are reactivated in shear. These fractures are seen either to terminate or originate at major stylolite surfaces, but cross-cut thinner, less well developed stylolites. They are typically partly cemented and may contain significant open aperture.

- Set 4 – Fractures originate as opening-mode and are rarely reactivated in shear. They post-date stylolites, often cutting and offsetting them. Like set 3 fractures, they have preserved open apertures and probably provide local connectivity across what would be considered flow boundaries with respect to matrix properties only.

Flow through fracture rock is controlled on a first order by average fracture apertures and connectivity. These two aspects are commonly difficult to measure and predict. Fracture density (inverse of spacing) is often used as a proxy for fracture connectivity. Predicting fracture spacing away from core-control requires determining the causes and controls on fracture formation and variability. Analysis of fracture sets relative to their causes in Cepu buildups shows that variations in mechanical rock properties are the primary control on fracture formation, with stylolitized bedding contacts ultimately controlling fracture heights. Fracture spacing is not directly related to carbonate litho-types (Figure 17), but is strongly correlated to porosity, meaning decreasing matrix porosity corresponds to decreasing fracture

spacing (or increasing fracture density). The porosity link results from changes in rock stiffness as pore space is filled with diagenetic calcite cements, the stiffer low porosity rocks fracture more easily than the high porosity rocks, all other factors being equal (Figure 18).
The amount of open-fracture aperture is the most important characteristic with respect to predicting fracture permeability. Many of the Cepu fractures observed in core have a large fraction of their surfaces still open to flow and are often solution-enhanced. An "effective aperture" is calculated as the average observed aperture (either filled or open) multiplied by the fraction of the fracture remaining open. This represents the average effective aperture available for flow. In the Cepu cores the mean effective aperture for all observed set 3 and set 4 fractures is approximately 0.2 mm, with some individual fractures having effective apertures as large as 1.3 mm. Thus the natural fractures have significant potential to affect flow where they form a connected system. The set 3 and set 4 fractures which post-date stylolite formation and matrix cementation are often solution-enhanced, again illustrating the strong linkage between fracture flow properties and chemical diagenetic events.

The detailed characterization data have two purposes. First, to understand the conceptual fundamental fracture controls that ultimately are used in a predictive sense, to populate fractures away from direct well control. Second, to develop a quantitative database for building frequency distributions used to model permissible, but non-unique field-wide fracture distributions based on a discrete fracture-network approach. Such models are conditioned to distribute fractures according to the observed statistical distributions constrained to the observed fracture-controlling lower porosity rocks. The result is a fracture permeability "overlay" with two important attributes; (1) the local matrix permeability may be enhanced by up to 2 orders of magnitude due to fracturing either confined between adjacent well developed stylolites or within laterally restricted low-permeability zones, (2) the vertical permeability of the lowest porosity rocks may be significantly increased over larger areas. This second effect leads increases in vertical connectivity as a function of the distribution of porosity-reducing diagenesis. If the porosity is low enough and the cemented zone extensive enough, the fractures can compromise no-flow barriers between flow units. This can have an impact on pressure drawdown in nearby wells and increase effective well-drainage volumes, thus improving recovery but at the expense of increasing potential for early water breakthrough.

Field Reservoir Simulation

This section focuses on simulations to characterize the field excess permeability including single and dual porosity and permeability models. To evaluate the range of impact of fracture on production, a dual porosity (DP) simulation model was constructed. In dual-porosity simulation, the matrix and fracture regions are modeled separately, using a dual-node grid. Each simulation cell is represented by two nodes, a matrix node and a fracture node, located at the same position in space but with different properties. In dual-porosity modeling, flow between adjacent simulation cells is calculated through the high-permeability fracture nodes; fluid exchange occurs between the matrix and fracture nodes as specified by the dual-porosity pseudo-functions. In addition to the usual structural and property model parameters normally supplied by the geologic model, dual porosity simulations require additional fracture properties, including fracture porosity, fracture permeability and fracture density / spacing (Lx, Ly and Lz). A Discrete Fracture Network (DFN, Figure 19) model was constructed, based on the results of fracture analysis, to provide fracture properties.

Although DP model is considered the most rigorous modeling technique available for fractures, the challenges are that it normally requires long simulation time, and more importantly, it needs significant amount of data for model verification and calibration. Considering the level of uncertainty pertaining to fracture properties, instead of building a deterministic DP model, a series of sensitivity cases were designed and tested to understand the flow behavior altered by fracture, and quantify the range of production impact. The testing conditions and results are summarized in Table 1. In these sensitivities, fractures were selectively limited within certain area, and different percentages of DP cells were "activated". The adjustments were readily implemented in the simulation model, which was constructed using ExxonMobil proprietary software, EMpower.

Figure 20 is a comparison of production profile between DP and SP (single porosity) model. In this example, fractures were limited in the platform margin and backstep areas, which are more prone to factures. As shown, gas production in DP model was higher because fractures provide high-permeability conduits for gas movement. Conversely, DP model had higher oil rate due to higher well productivity attributed to excess permeability. Also, water rate was lower because of lower drawdown from wells. This example highlighted two competing factors affecting field production. Fractures could be beneficial for recovery as they enhanced fluid movement and well productivity through excess permeability. However, when fractures are pervasive such as Case 1, they became a production threat because gas and water breakthrough were accelerated through high-permeability, low-porosity fracture conduits, resulting in high gas and water rate. As shown in Table 1, depending on the percentage and area of DP cells, production (judged by the length of plateau and EUR) in DP model could be improved or poorer than SP model. The range of difference was -20 ~ +3 months in plateau, and -44 to +50 MSTB in EUR, estimated at the end of PSC term.

As mentioned previously, the limitation of DP models is long simulation time and high uncertainty. For B-field application, it was decided that a conventional single porosity model is appropriate for development support and regular business need. Based on the results of fracture analysis and available production data, it was further determined that in Case 2.2 10% of DP cells in backstep and margin area was the most likely scenario. The results of Case 2.2 will be used as a bench-mark to calibrate single porosity model. The remaining challenge was to represent DP effects in single porosity models. This was accomplished by pseudo-wells and permeability enhancement.

References

Apotria, T., M.A. Weidmer, D. Walley, A.Derewetzky and D. Millman, 2009, Mass wasting and detrital carbonate deposition, Cepu Block, East Java: Proceedings, Indonesian Petroleum Association, 33rd Annual Convention and Exhibition, 9 p.

Ardhana, W., 1993, A depositional model for the Early Miocene Ngrayong Formation and implications for exploration in the East Java Basin: Proceedings of the 22nd Annual Convention, Indonesian Petroleum Association, v. 1, p. 395-443.

Bransden, P.J.E., and S.J.Matthews, 1992, Structural and stratigraphic evolution of the East Java Sea, Indonesia: Proceedings, 21st Annual Convention, Indonesian Petroleum Association, v. 1, p. 417- 453.

Cole, J.M,. and S. Crittenden, 1997, Early Tertiary basin formation and the development of lacustrine and quasi-lacustrine/marine source rocks on the Sunda Shelf of SE Asia, in A.J. Fraser, S.J. Matthews, and R.W. Murphy, (eds.), Petroleum Geology of Southeast Asia: Geological Society of London, Special Publications, v. 126, p. 147-183.

Najoan, G.A.S., 1972, Correlation of the Tertiary lithostratigraphic units in the Java Sea and adjacent areas: Proceedings, 1st Annual Convention, Indonesian Petroleum Association, p. 11-16.

Prasetyadi, C., E.R. Suparka, A.H. Harsolumakso, and B. Sapiie, 2005, Eastern Java basement rock study: preliminary results of recent field study in Karangsambung and Bayat areas: Proceedings, 34th Annual Convention, Indonesian Association of Geologists, p. 310- 321.

Smart, P.L., R.J. Palmer, F. Whitaker, and V.P. Wright, 1988, Neptunian dikes and fissure fills: An overview and account of some modern examples, in N.P. James, and P.W. Choquette, (eds.), Paleokarst: New York, Springer-Verlag, p. 149–163.

Soeparyono, N., and P.G. Lennox , 1989, Structural development of hydrocarbon traps in the Cepu Oil field Northeast Java, Indonesia: Proceedings, 18th Annual Convention, Indonesian Petroleum Association, v. 1, p. 139-156.

Van Bemmelen, R.W., 1949, The geology of Indonesia: Government Printing Office, Martinus Nijhoff, The Hague, 732 p.

Van Simaeys S., A. Derewetzky, F. Musgrove, R. Sekti, T. Simo, N. Stephens, A. Weidmer, and A. Zeiza, 2011, Early carbonate growth in the East Java Basin, Indonesia; a case study from the Jambaran Field: Proceedings, 34th Annual Convention, Indonesian Petroleum Association, v. IPA11-G-205, 13 p.
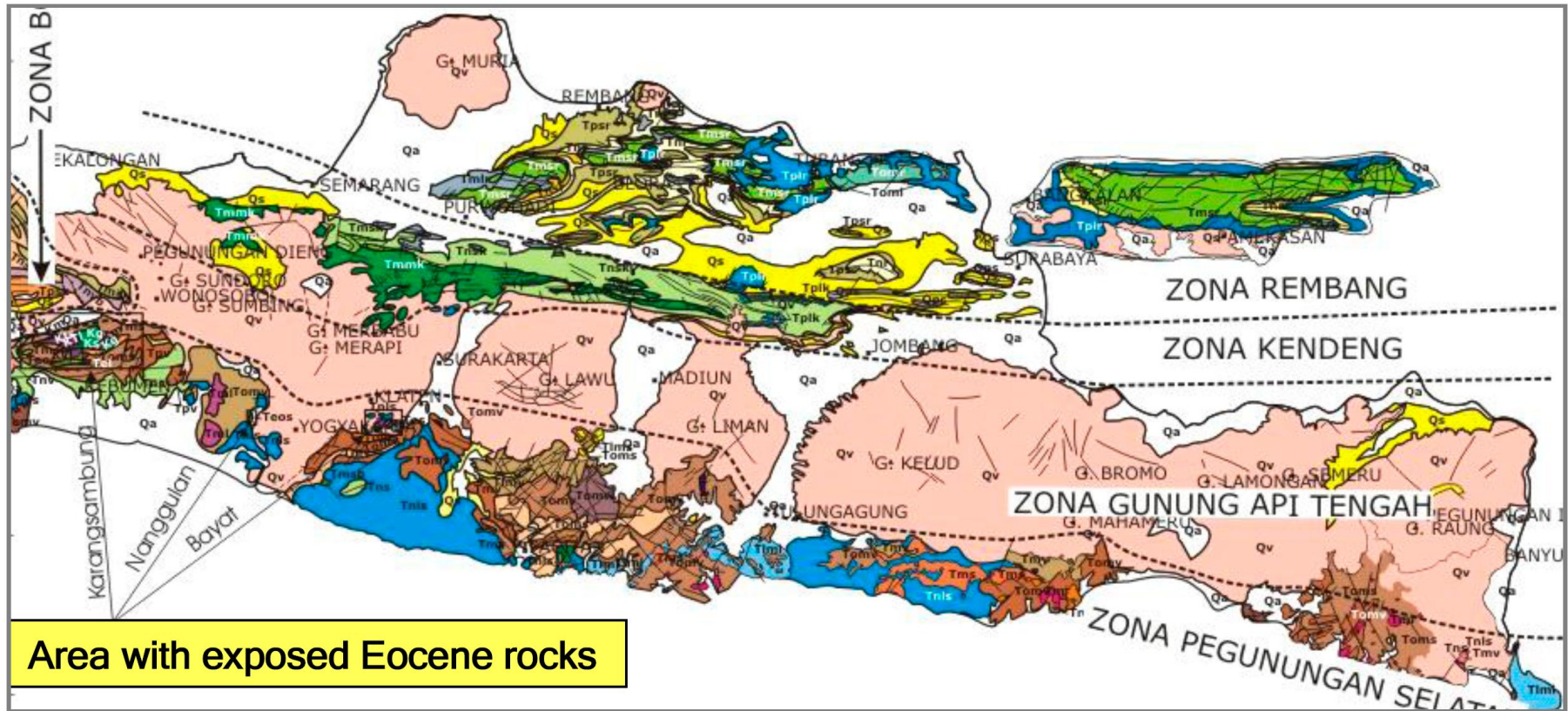
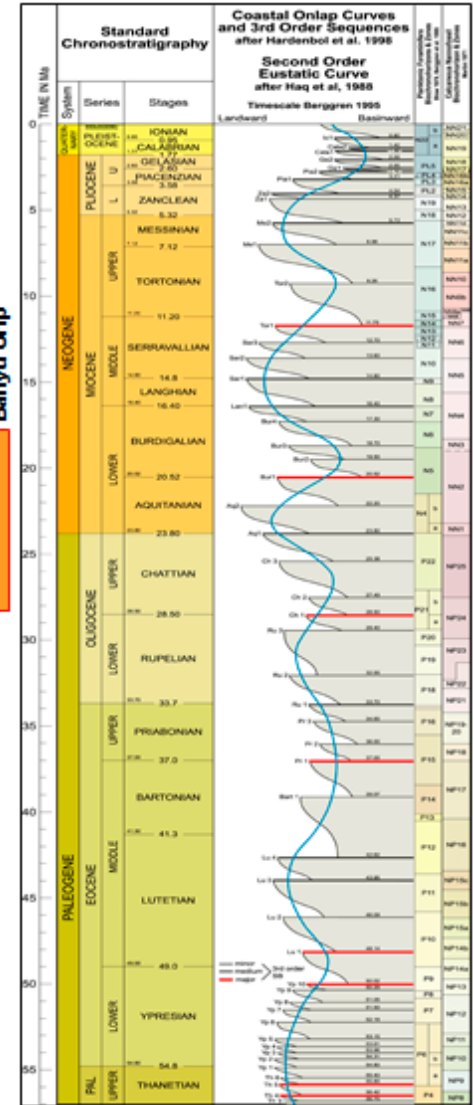Figure 1. Onshore East Java main structural domains (Prasetyadi et al., 2005, after Van Bemmelen, 1949).
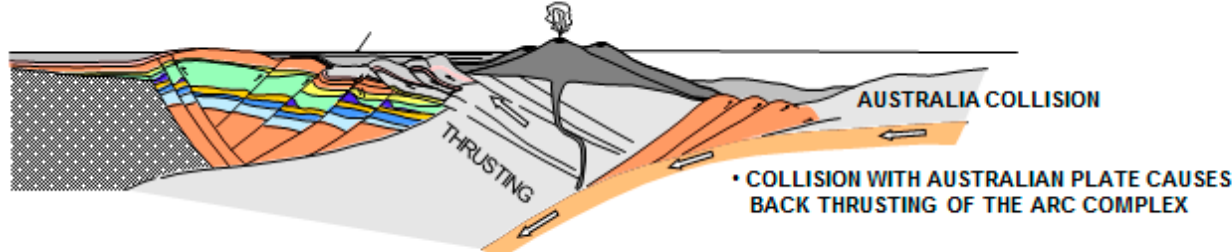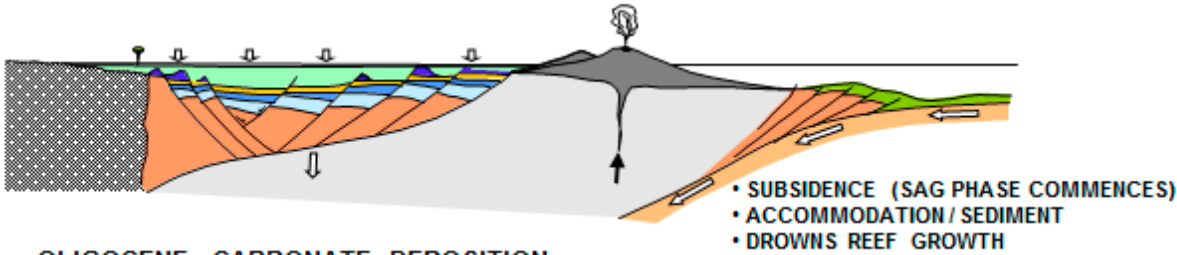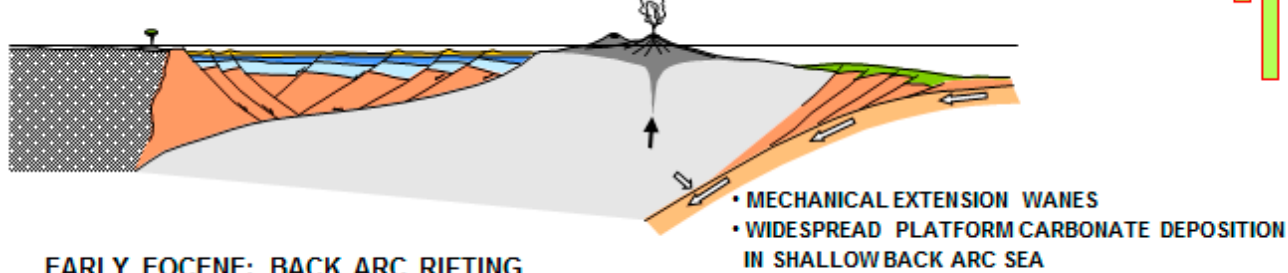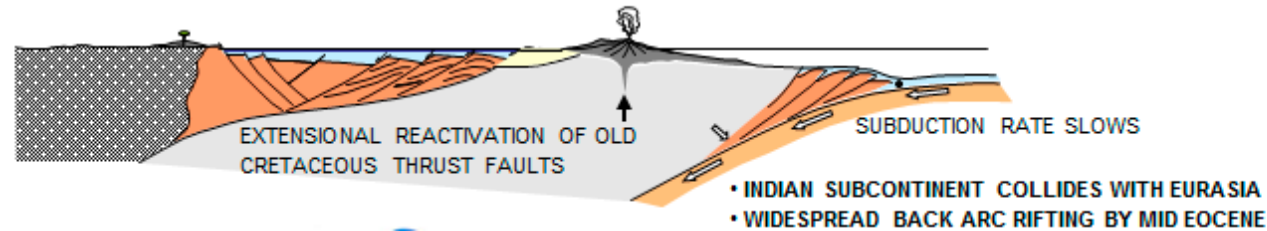
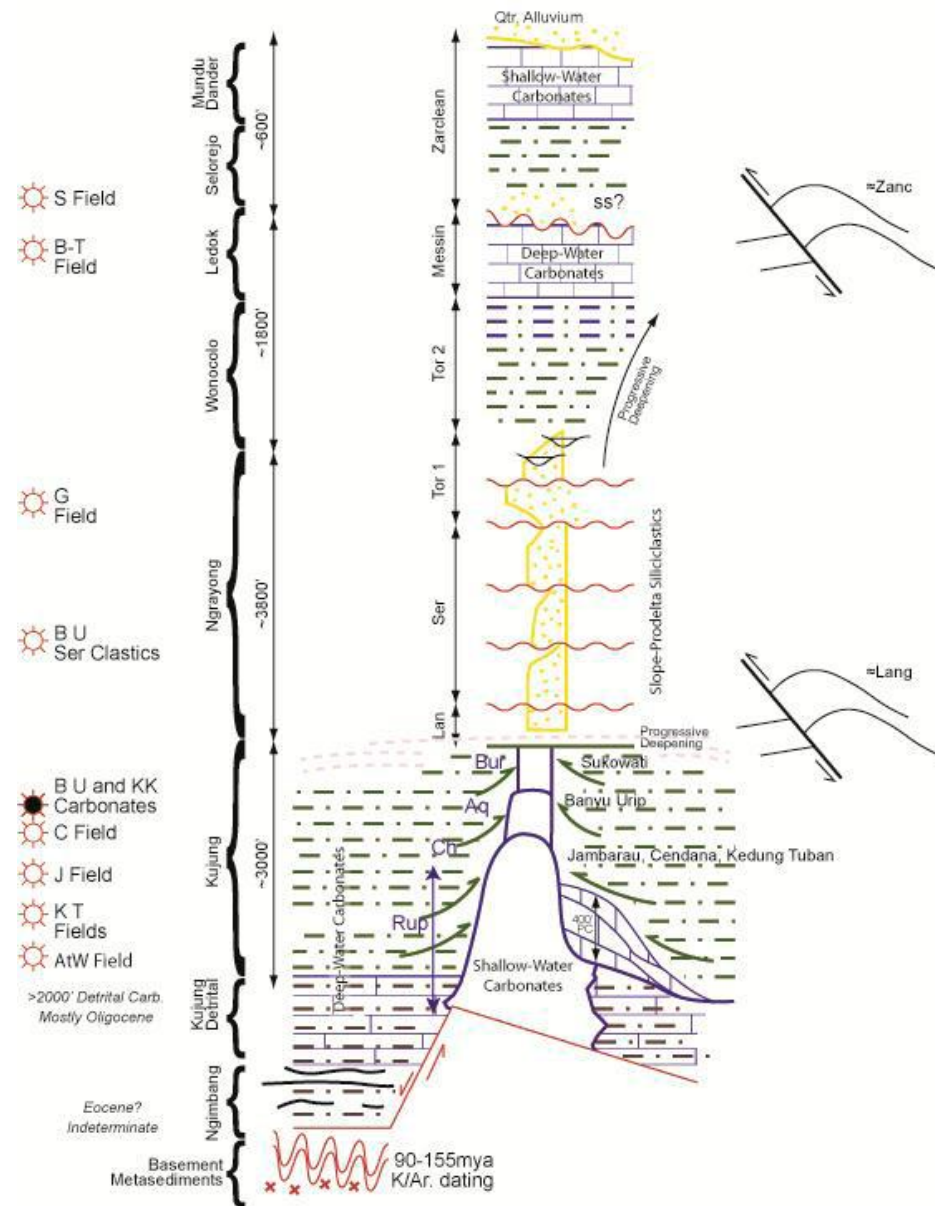Figure 2. East Java basin structural evolution.

Figure 3. Main stratigraphic units in the Cepu block, reservoir in some of the main oil and gas fields in the area (Soeparyono and Lennox, 1989), and the main structural events.
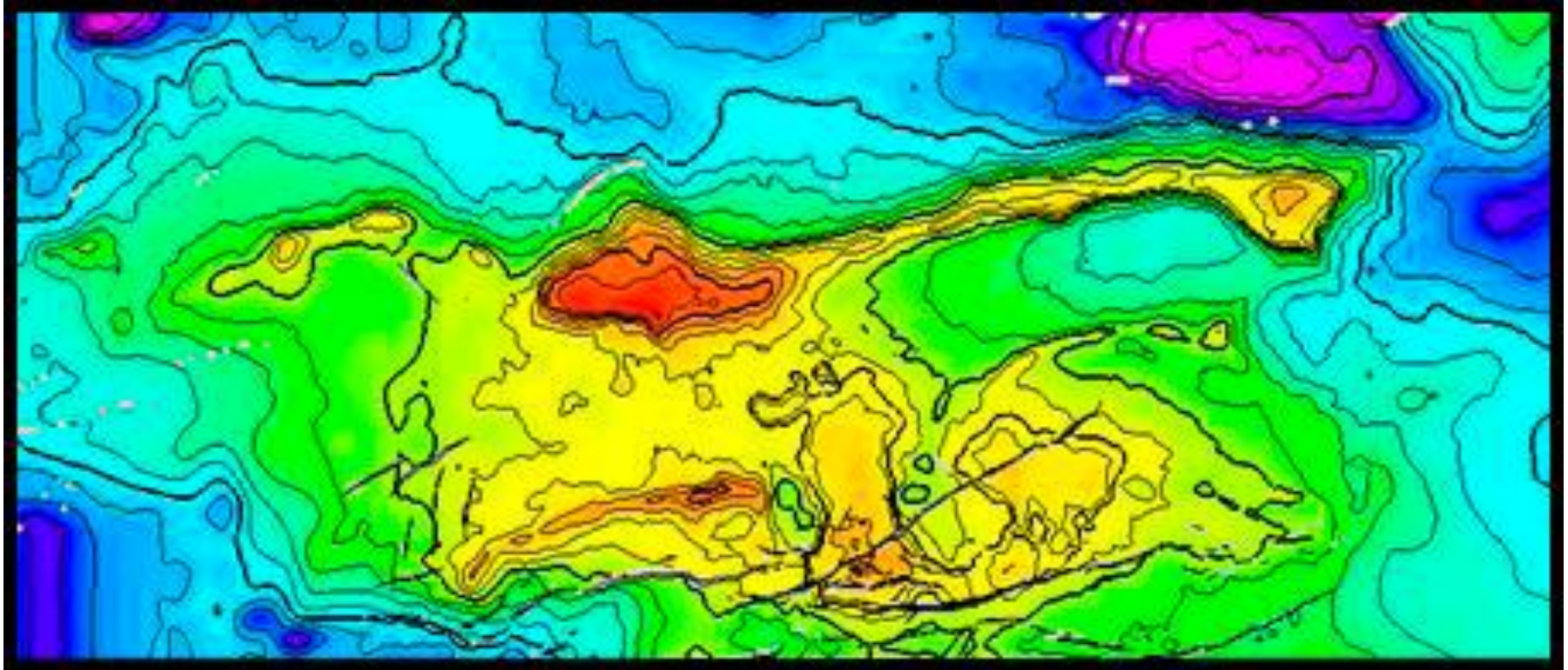
Figure 4. Top of the carbonate interval highlighting the different isolated carbonate platforms(culminations with warmer color) in the Cepu block.
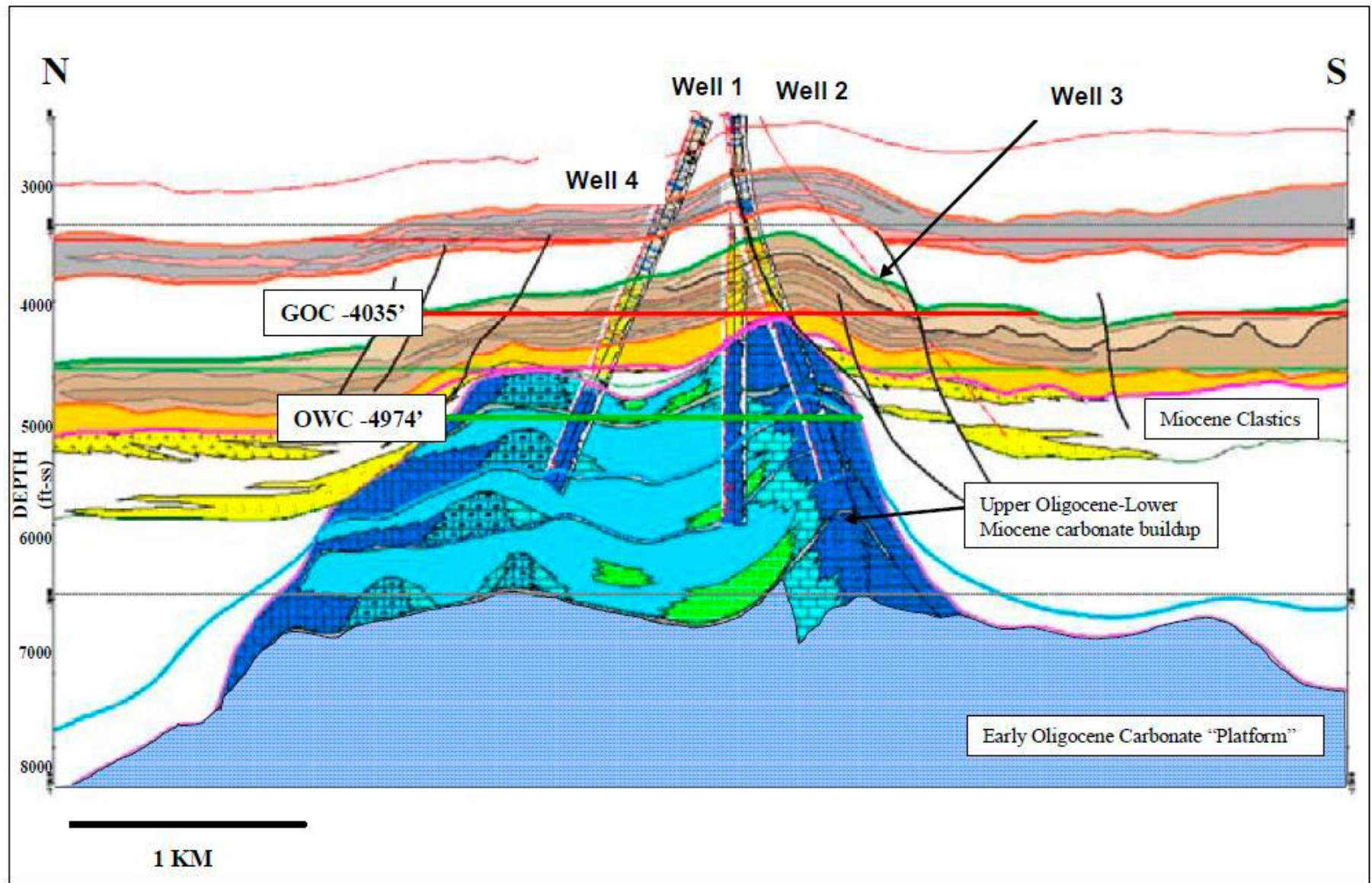
Figure 5. Banyu Urip oil field with the key (carbonate and siliciclastic) reservoirs.
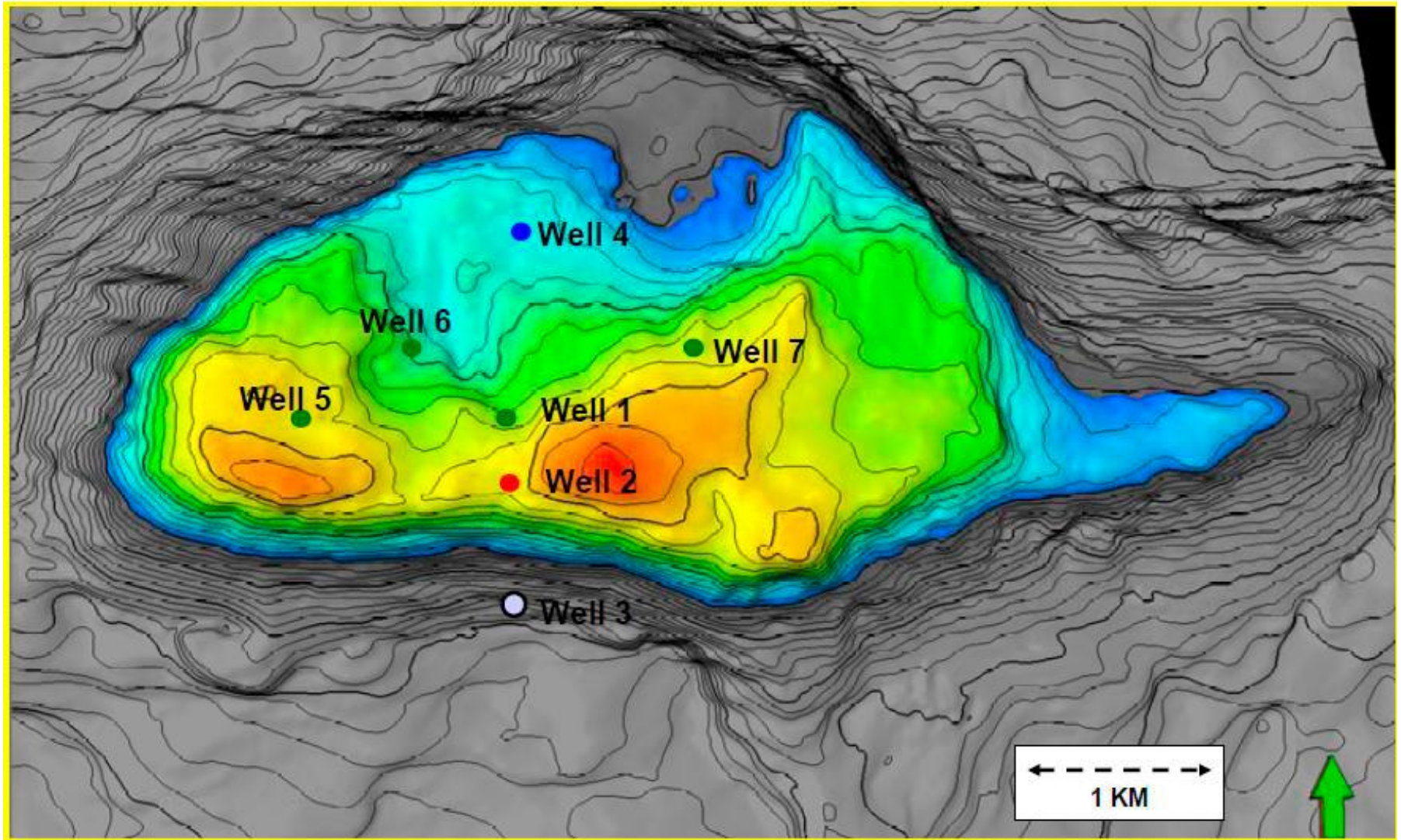
Figure 6. Top of Banyu Urip Field and location of wells discussed in the text.
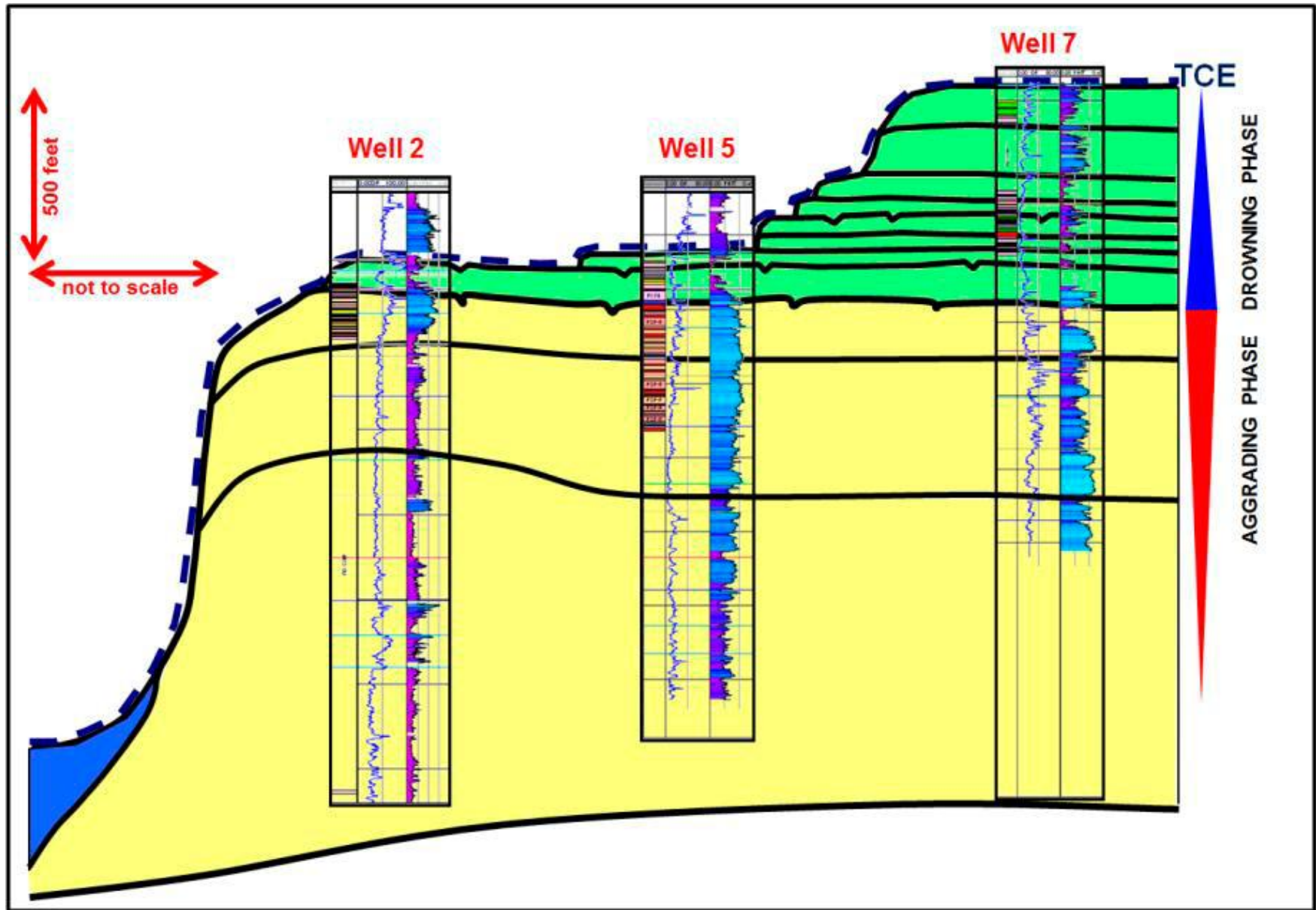
Figure 7. Stratigraphic summary of the Chattian-Burdigalian, Banyu Urip, with an aggrading phase (yellow) and retrograding phase (green). Also notice the deep-water facies (blue) onlapping the slopes of the carbonate buildup.
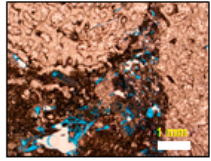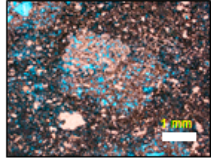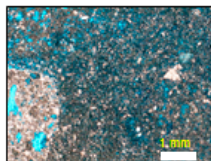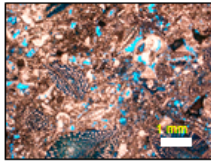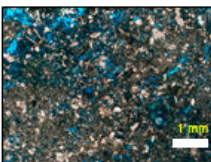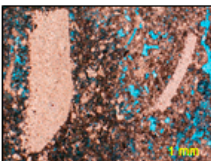
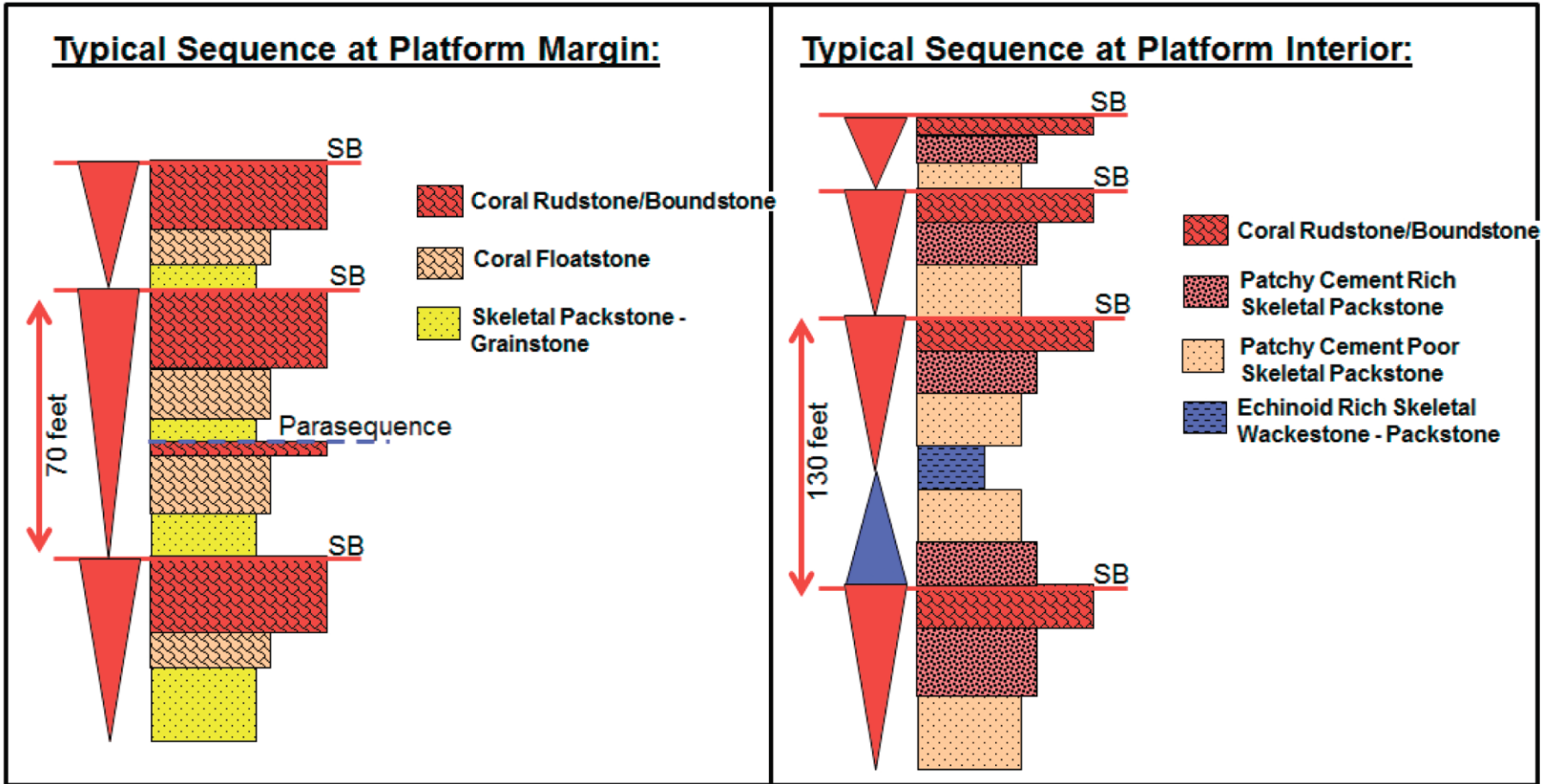|	Lithofacies	Texture	Reservoir Characteristics	Common Features	Depositional Environment	Thin Section Photos
1	Coral Boundstone / Coral Rudstone CB/CR	Matrix: P to MLP	• Low to moderate porosity. • Low to permeability permeability. • Pore types: Touching Vugs and enhanced moldic abundant porosity and; minor microporosity, and interparticle porosity.	• Coral rich facies. Abundant biotas: corals and coral fragments, encrusting red algae and foraminifera on corals, large benthic foraminifera (LBF), gastropods and echinoderms. Minor red algae fragments. • High/abundant recristalization of corals. • Bladed isopachous rim early marine cement.	• Shallow subtidal, moderate to high-energy, above fair weather wave base. • Platform Margin or Platform Interior (Patch Reefs).	
2	Patchy Cemented Skeletal Packstone - Rich PSP-R	Matrix: P	• Moderate to high porosity • Moderate to high permeability • Pore types: Enhanced Moldic and microporosity abundant.	• Skeletal packstone with abundant distribution of patchy cemented rock. • Dominant biotas: large benthic foraminifera (LBF), echinoderms, pelloids, and minor coral fragments. • Moderately sorted. • Bladed isopachous rim early marine cements.	• Shallow subtidal, moderate-energy, at fair weather wave base. • Platform Interior.	
3	Patchy Cemented Skeletal Packstone - Poor PSP-P	Matrix: P to W	• High porosity • High permeability • Pore types: Microporosity and enchanced moldic abundant.	• Skeletal wackestone - packstone with rare to common distribution of patchy cemented rock. • Dominant biotas: large benthic foraminifera (LBF), echinoderms, pelloids, and minor coral fragments. • Moderately sorted. • Bladed isopachous rim early marine cements.	• Shallow subtidal, moderate-energy, at fair weather wave base. • Platform Interior.	
4	Skeletal Packstone to Grainstone SPG	Less common: G	• Low to high porosity. • Low to high permeability. • Pore types: interparticle and moldic porosity abundant; minor intraparticle porosity.	• Large benthic foraminifera (LBF), echinoderms, bivalve fragments, and gastropods. • Moderate – well sorted. • Grain size vary from fine to coarse. • Blocky calcite cements. • Commonly preserve primary porosity.	• Shallow subtidal, high-energy, above fair weather wave base. • Platform Margin (Shoals) or Platform Interior (Shoals).	
5	Skeletal Wackestone to Packstone SWP	W to P	• high porosity. • high permeability. • Pore types: microporosity and enhanced moldic abundant.	• Fine-grained skeletal fragments. • Dominant biotas: benthic foraminifera, sponge spicules and unidentified sekeletal fragments. • Moderate – well sorted. • Bioturbated.	• Deeper subtidal, low-energy, below fair weather wave base. • Platform Interior (deeper part).	
6	Echinoid Wackestone to Packstone EWP	W to P	• High porosity. • High permeability • Por types: Microporosity and enhanced moldic.	• Dominant biotas: echinoderm, large benthic foraminifera (LBF), skeletal fragments, and red algae fragments. • Poorly sorted. • Bioturbated. • Abundant leaching.	• Deeper subtidal, low-energy, restricted, below fair weather wave base. • Platform Interior (deeper part).	

Figure 8. Typical facies in the aggrading phase.

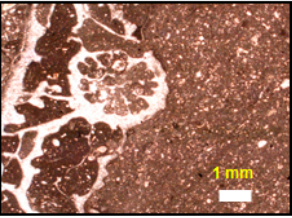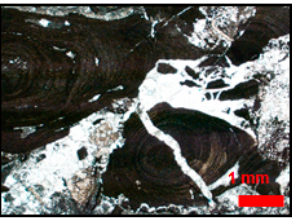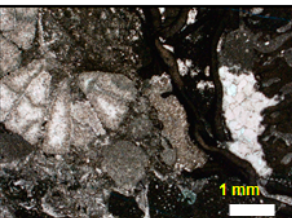Figure 9. Typical sequences of aggrading phase at margin and platform interior.

	Lithofacies	Texture	Reservoir Characteristics	Common Features	Depositional Environment	Thin Section Photos
1	Platy Coral Floatstone to Bafflestone **PCFB**	*Matrix:* P to W	• Low to high porosity. • Low to high permeability • Moldic, vuggy and microporosity; minor fracture porosity.	• Platy corals, delicate finger coral fragments, platy and encrusting red algae, echinoderms, planktonic foraminifera, and minor large benthic foraminifera (LBF). • Poorly sorted. • Bladed isopachous rim early marine cement.	• Deeper subtidal, low to moderate-energy, at and below fair weather wave base. • Platform Interior (deeper part).	
2	Rhodolith Floatstone to Rudstone **RFR**	*Matrix:* P	• Low to moderate porosity • low to moderate permeability. • minor fracture porosity.	• Red algae (Rhodoliths), encrusting red algae on corals, large benthic foraminifera (LBF), echinoderms, and gastropods. • Poorly sorted.	• Shallow to deep subtidal, moderate-energy, at and below fair weather wave base. • Platform Interior (shallow to deeper part).	
3	Platy Red Algae Floatstone to Bafflestone **PRAFB**	*Matrix:* P	• Low porosity. • Low permeability. • Microporosity; minor fracture porosity.	• Platy and encrusting red algae, platy coral fragments, planktonic foraminifera, minor large benthic foraminifera (LBF), bivalves, and echinoderms. • Poorly sorted. • Blocky calcite cements.	• Deeper subtidal, low-energy, below fair weather wave base. • Lower Slope or Platform Interior (deeper part).	

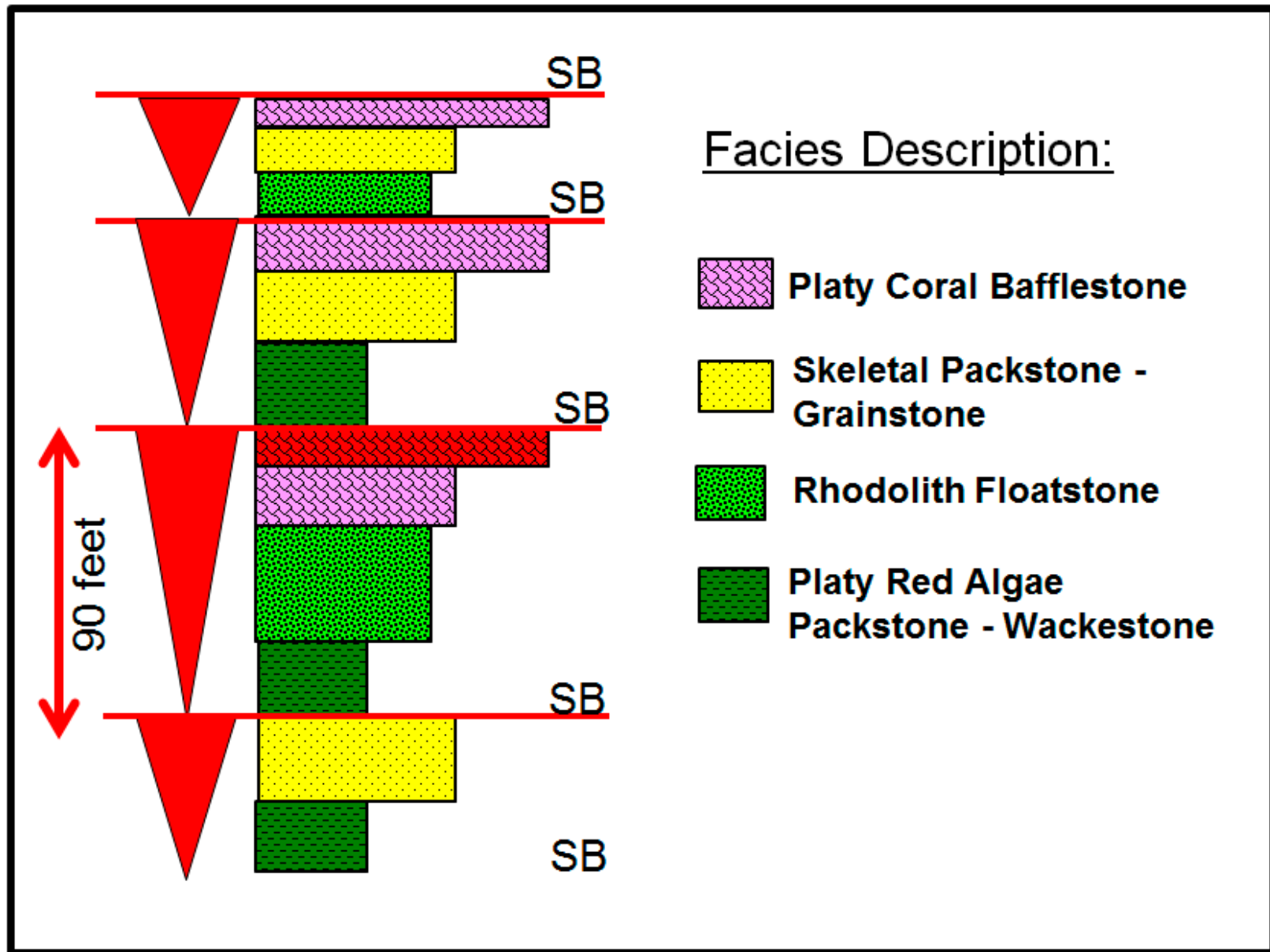Figure 10. Typical facies in the retrograding phase.

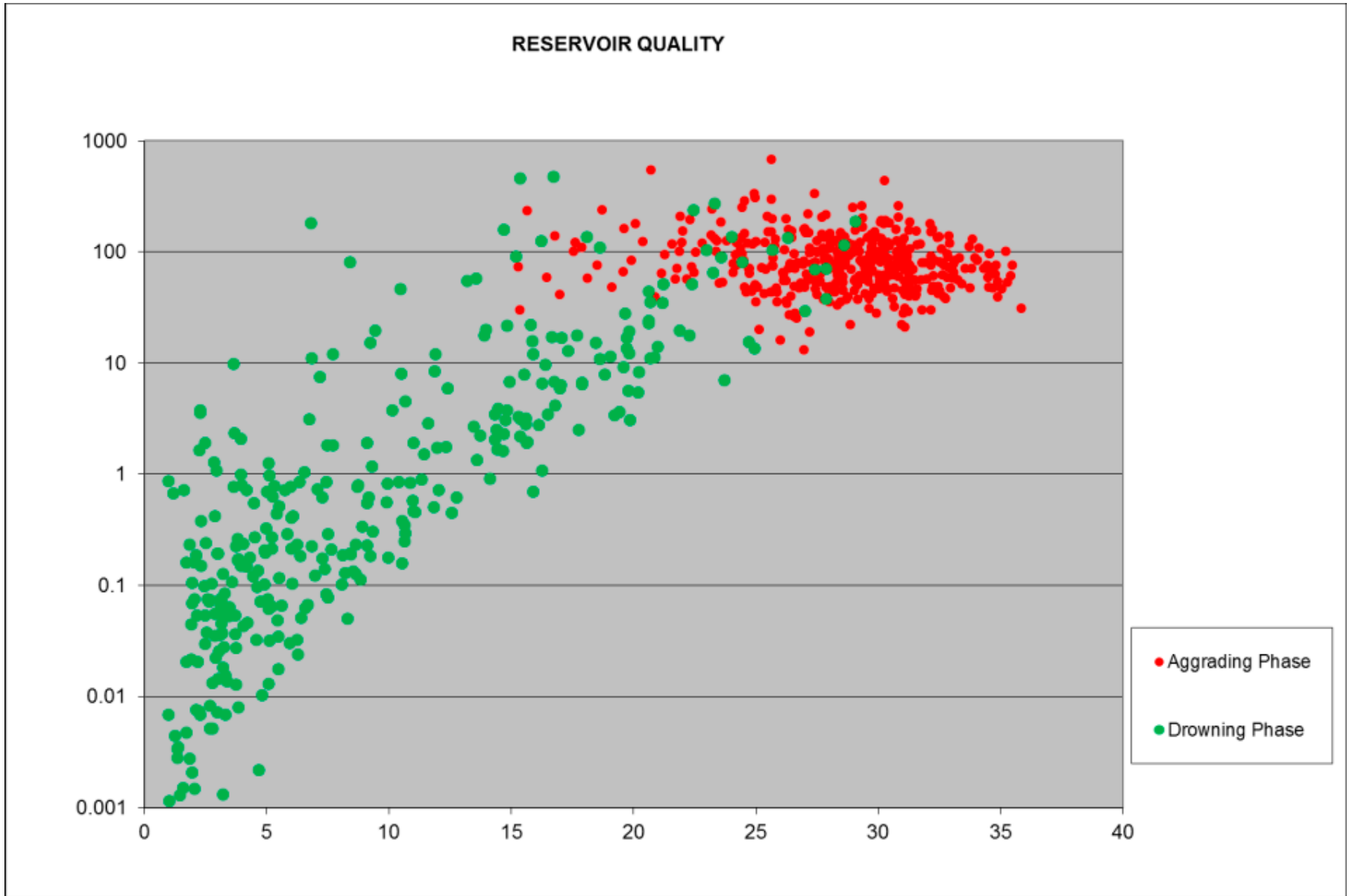Figure 11. Typical sequences for the retrograding phase.

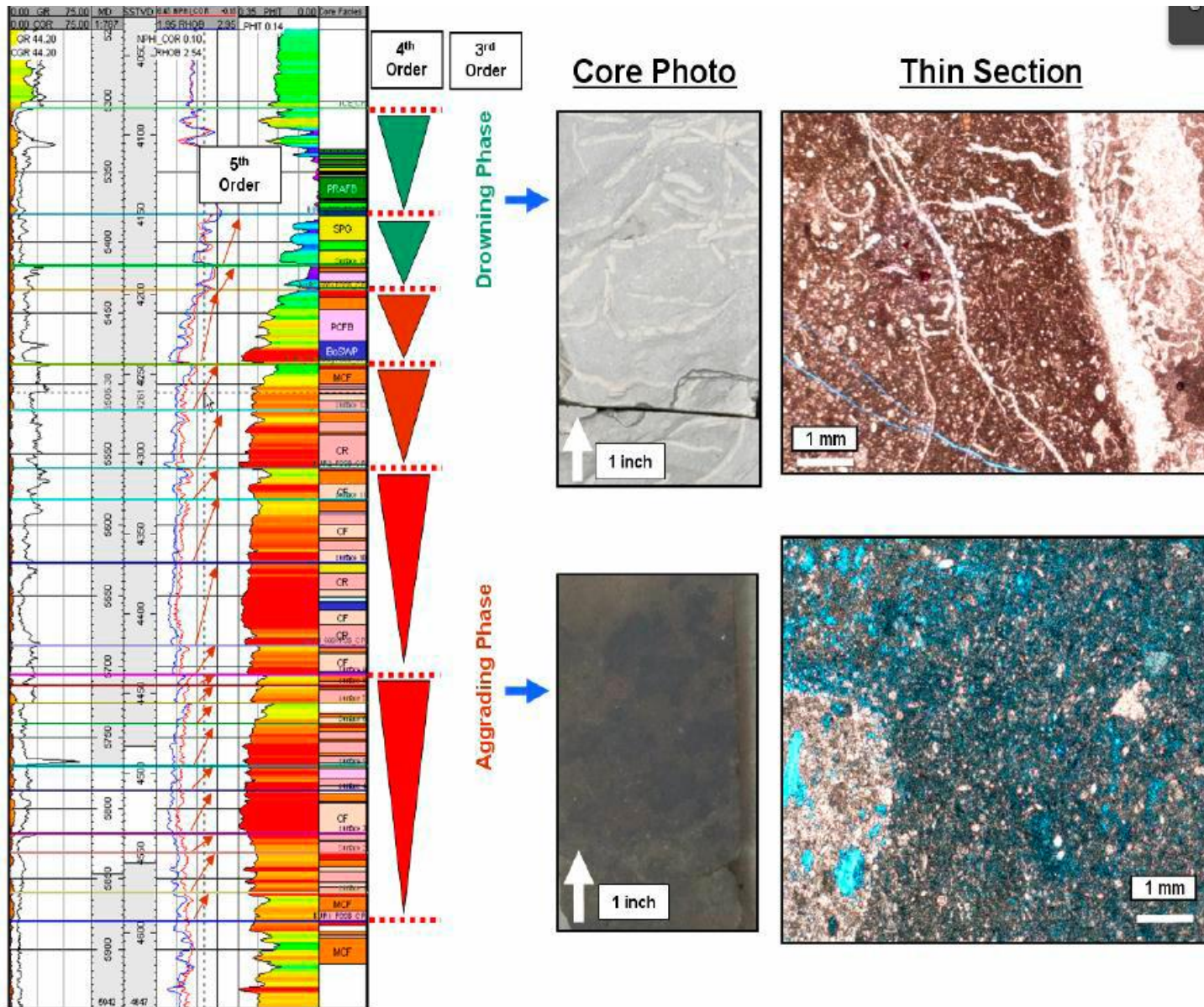Figure 12. Cross plot between porosity and permeability according to aggrading and retrograding phases.

Figure 13. A platform interior well showing the changes in porosity and permeability in the reservoir.

Diagenetic Process	Early	Shallow Burial	Late
Marine Cementation			
Micritization/Boring			
Local Vadose Cementation			
Exposure Related Fabric Destructive Dissolution			
Isopachous Fresh Water Phreatic			
FW Phreatic Inversion			
FW Phreatic Overprint			
Mixing Zone Leaching			
Syntaxial Overgrowths (Echinoids)			
Aragonite Leaching and Recrystallization			
Mechanical Compaction/Grain Breakage			
Microcrystalline Stabilization (Microporosity)			
Local Pervasive Matrix Dolomitization			
Stylolitization			
Calcite Cementation Related to Pressure Solution			
Disseminated Quartz, Silica Cements			
Fracturing			
Aggressive Dissolution 1			
Coarse Calcite Cements			
Hydrothermal Dolomite Cements			
Aggressive Dissolution 2			
Kaolinite Cements			
Aggressive Dissolution 3			
Microcrystalline Enhancement (Microporosity)			
Red Algae/Foram Dissolution			
HC Charge			

Figure 14. Paragenetic sequence.
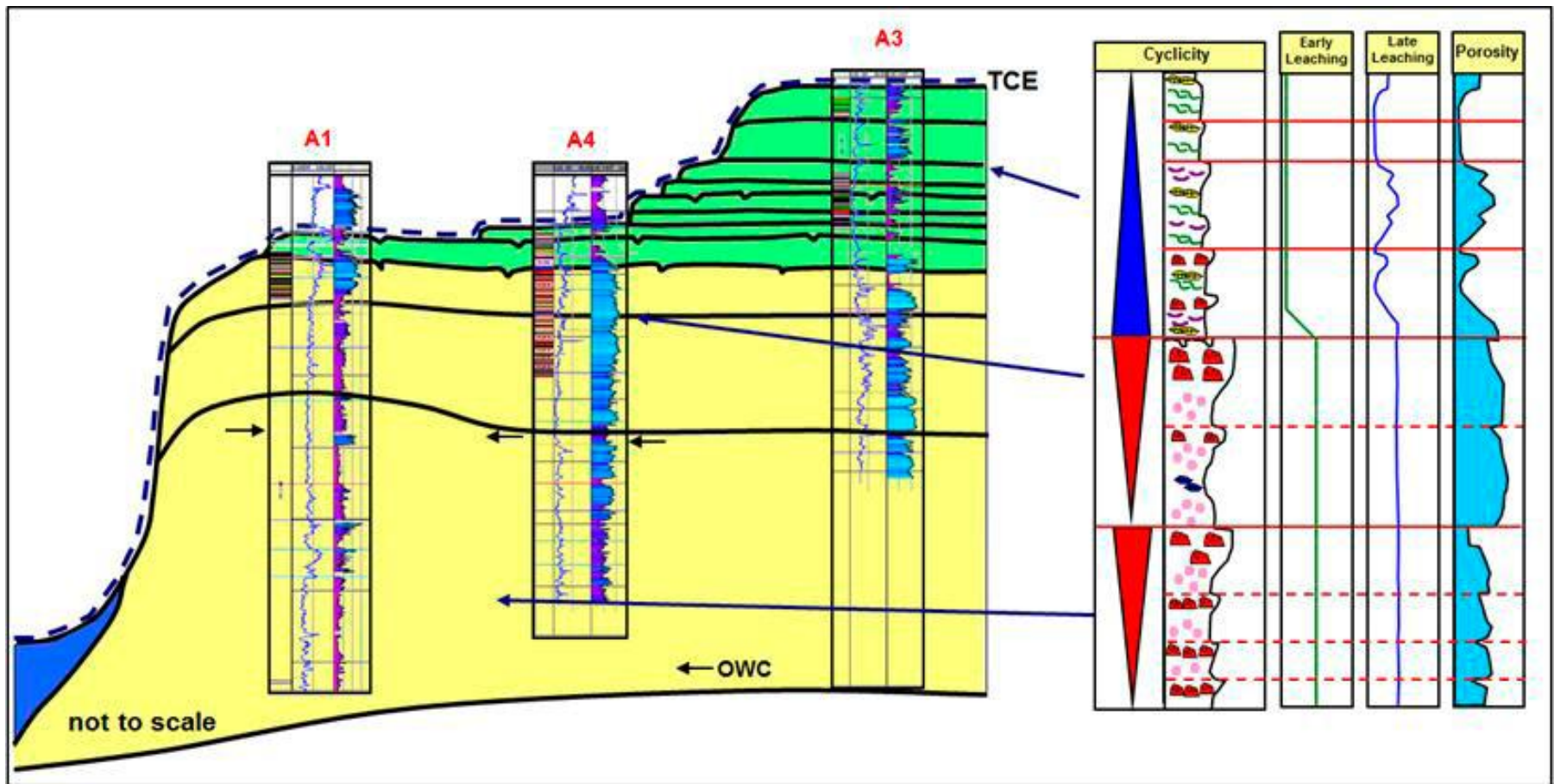
Figure 15. Summary of the diagenetic processes affecting Banyu Urip. See Figure 6 for well location.

Type I

- Length: cm's to meters
- Often canabalized by stylolites
- Usually nearly 100% filled
- Probably insignificant flow potential

Type II

- Length: 1 to 5 cm
- Usually bounded between adjacent stylolites
- Perpendicular to stylolite teeth
- Often solution enhanced forming "mega-pores"
- Local perm multiplier

Type III

- Length: ~cm to meter
- Often low angle to stylolites
- Cut stylolites and / or terminate on Type II fractures
- Often solution enhanced, may form continuous clusters.
- Significant for flow

Type IV

- Length: ~1 to 10's m (?)
- Cross-cut all but thickest stylolites
- Usually open, up to several mm's aperture
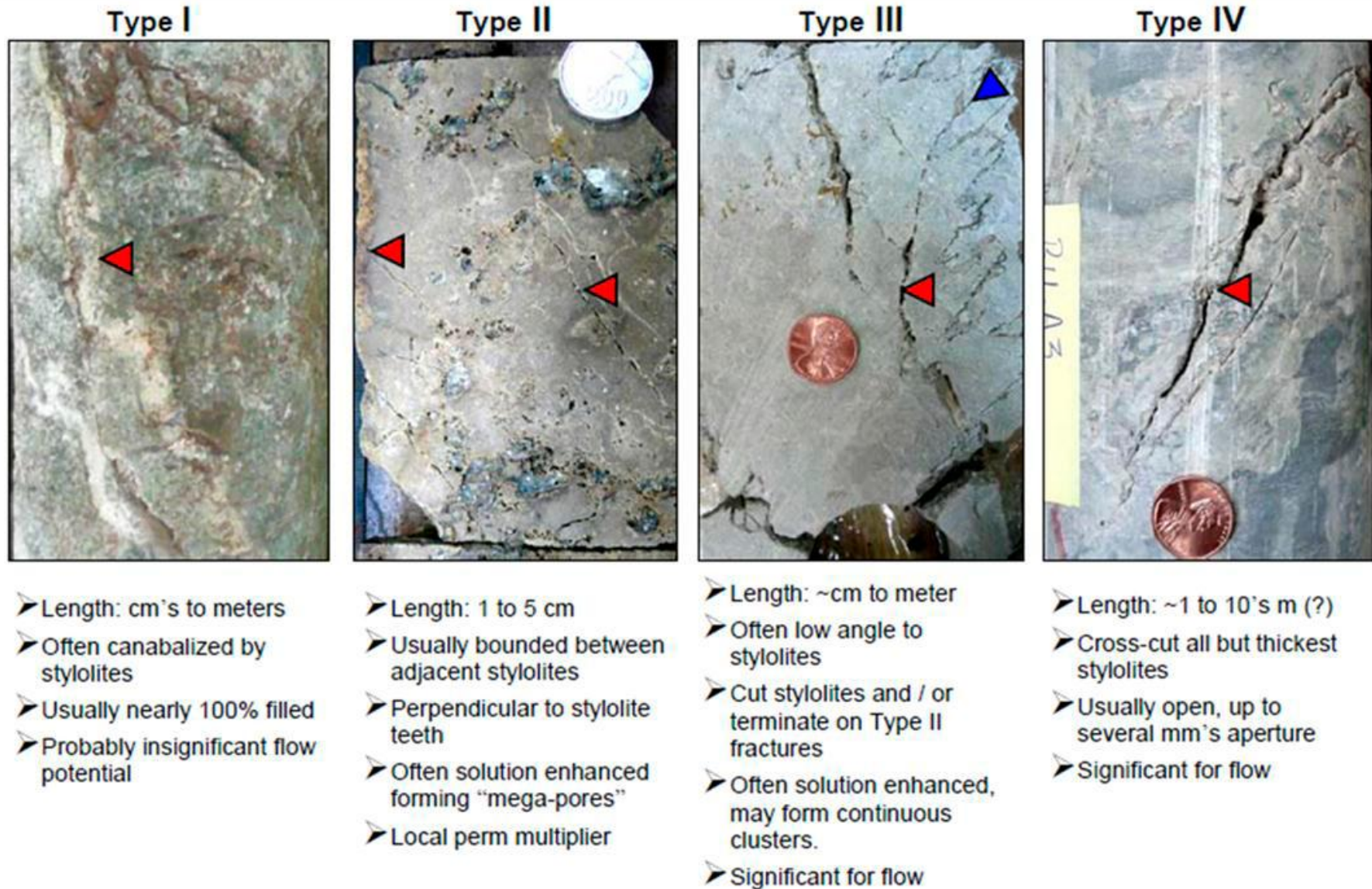- Significant for flow

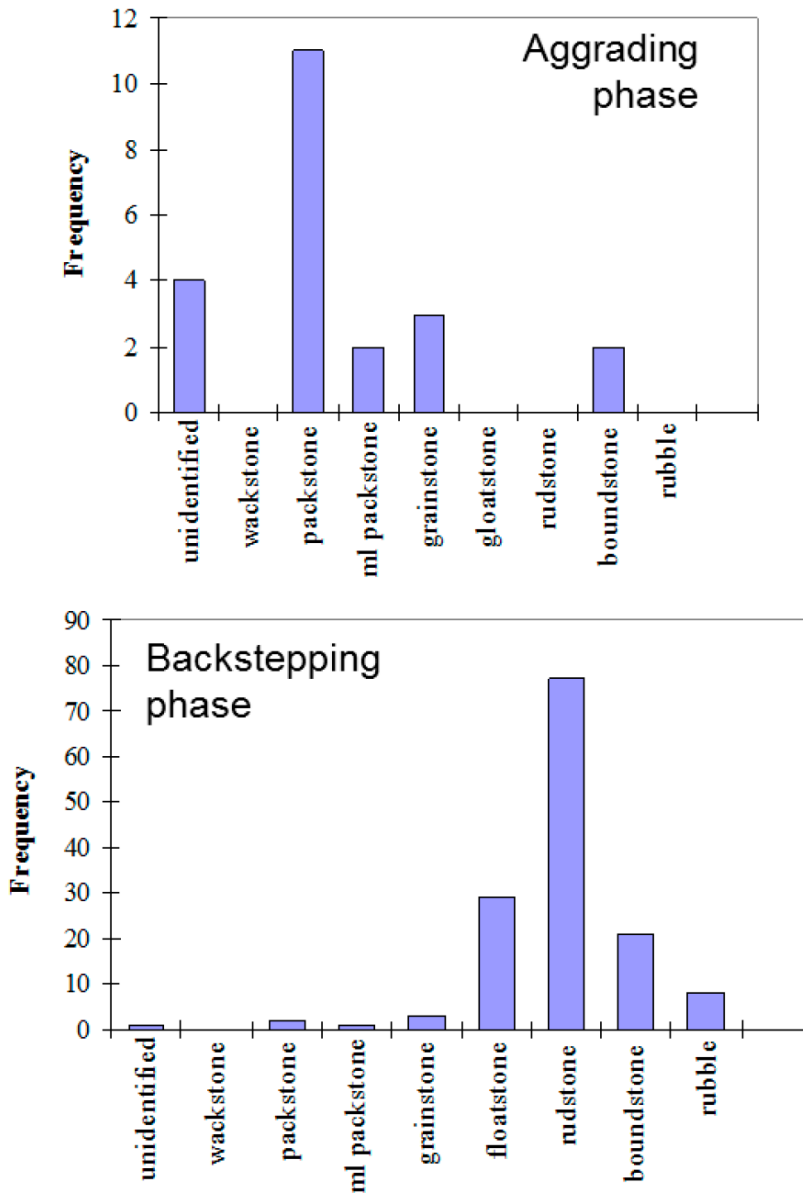Figure 16. Banyu Urip fracture types described in the text.

Figure 17. Fracture frequency observed in different lithofacies. Few rudstones were observed in the platform margin well, but packstones were plentiful in both wells. The distributions suggest that lithofacies type alone is not the dominant fracture control.
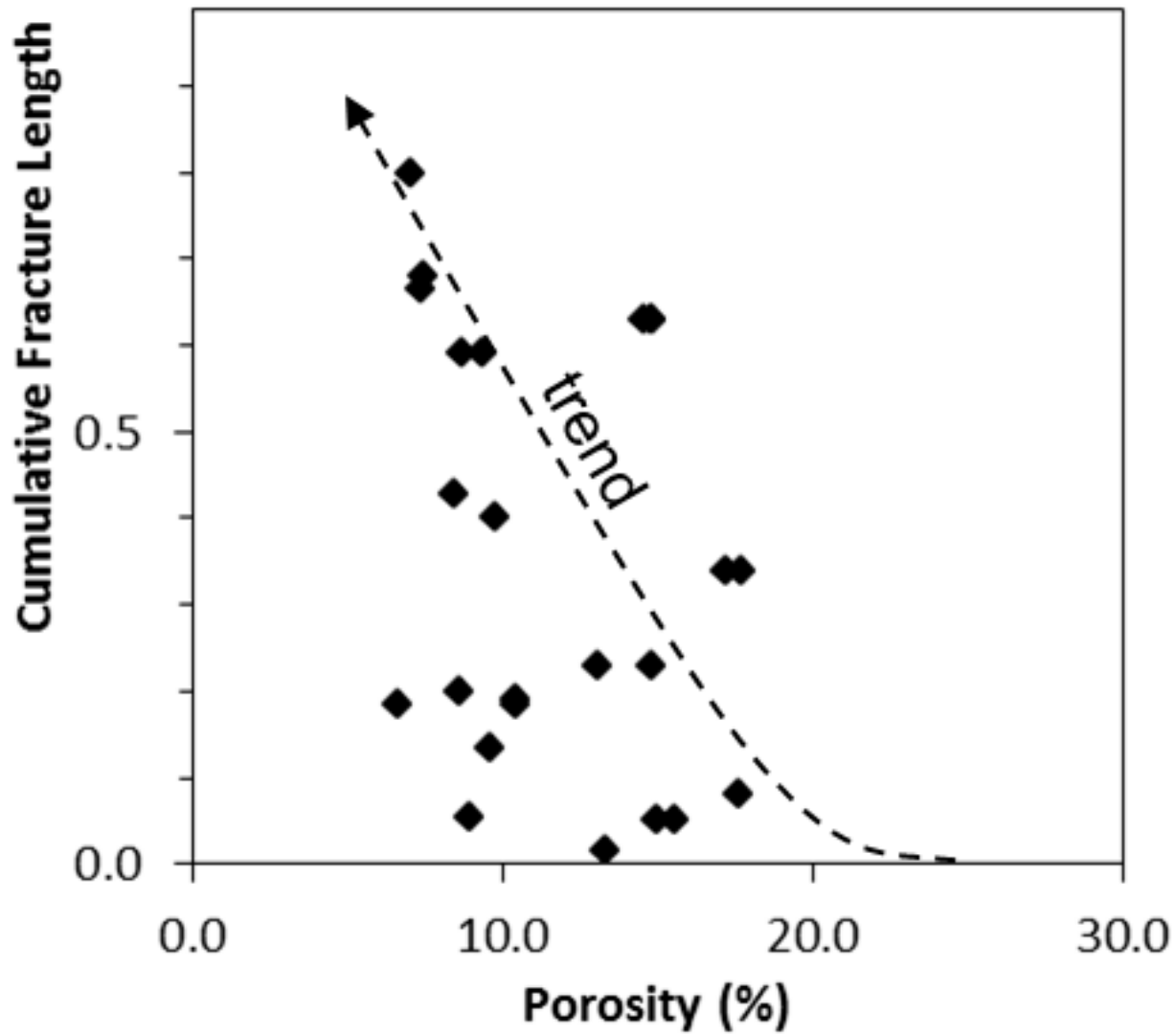
Figure 18. Cumulative fracture length (one=foot bins) verses matrix porosity for core from a well near the platform margin. Measured maximum fracture lengths show increase as porosity decreases, with some anomalies. Low porosity/low fracture-length points are probably due to sampling biases (high-angle well coring high-angle fractures)
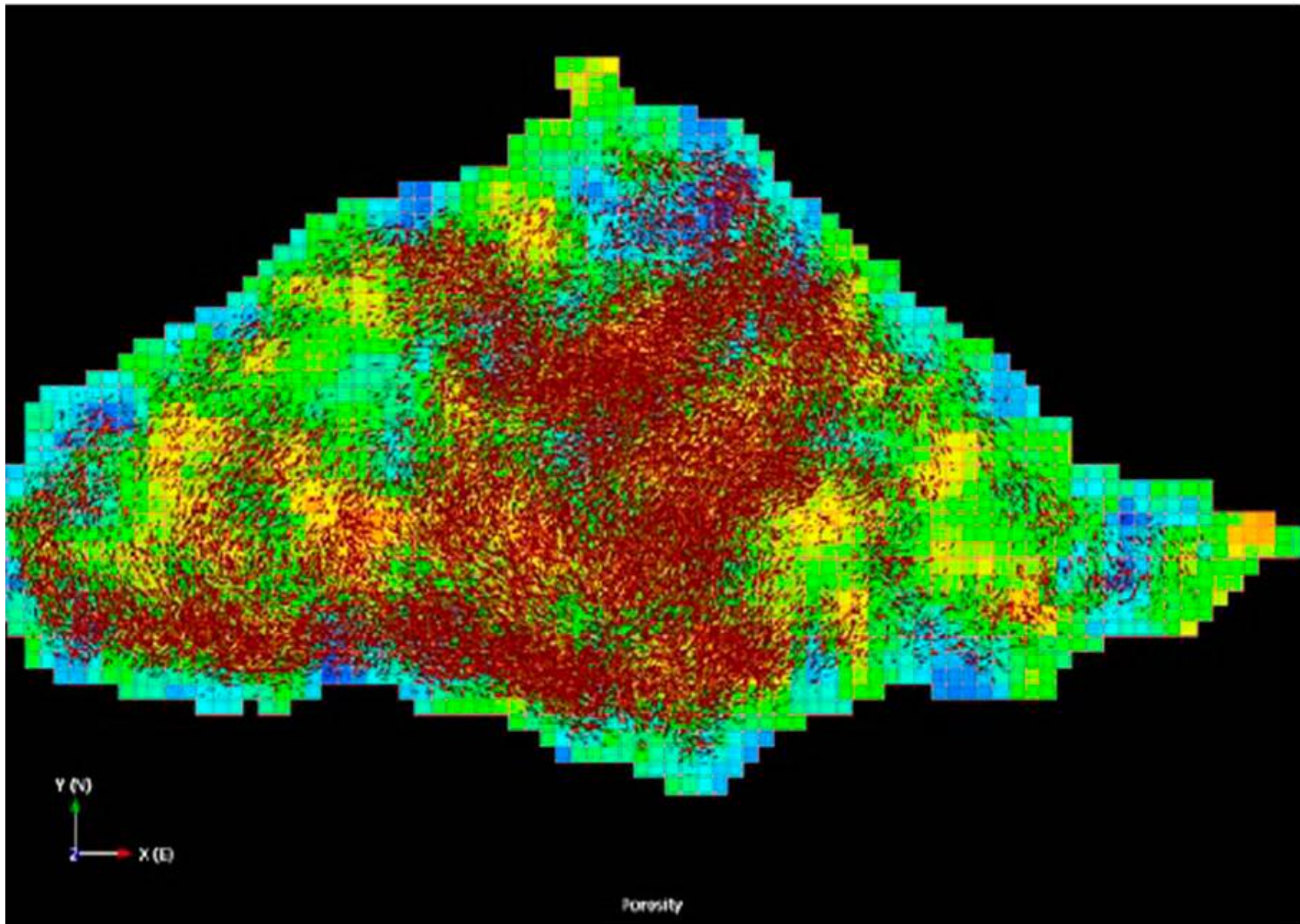
Figure 19. Discrete Fracture Network model for Banyu Urip. Notice the higher density of fractures (brown) at the margin and the backstepping region.
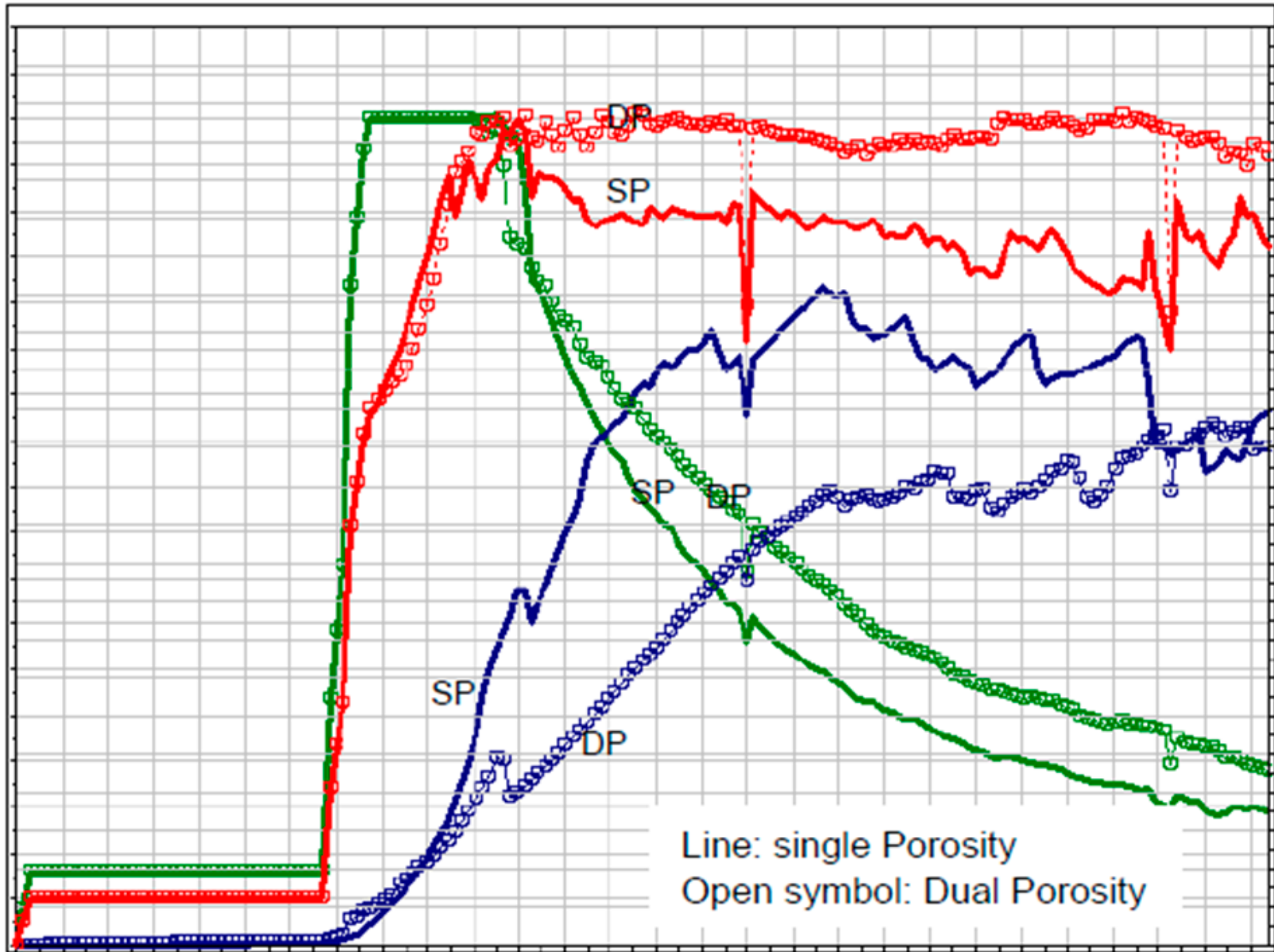
Figure 20. Comparison between production profiles between Single (SP) and Dual (DP) porosity Models (Green: oil rate; Red: gas rate; Blue: water rate).

		% of Active Dual Porosity Cells			Δ Plateau*	Δ EUR*
		BS / Margin	Low ϕ cells in platform interior	Others		
Case 1	DP in entire model	100	100	100	-20	-44
Case 2	DP in BS / Margin	100	0	0	-4	52
Case 2.1	30% DP in BS / Margin	30	0	0	3	35
Case 2.2	10% DP in BS / Margin	10	0	0	0	15
Case 2.3	Well connect to 30% of fracture blocks (reduced PI)	100	0	0	2	48
Case 3	Limited DP	30	15	5	3	50

*: the difference is in reference to the single porosity model

Table 1. Dual porosity model testing conditions and results.